Desalination and Water Treatment
www.deswater.com

doi: 10.5004/dwt.2017.20521

71 (2017) 261–270
April

Toward energy efficient reverse osmosis polyamide thin-film composite membrane based on diaminotoluene

Mohamed Said[a,b,*], Shaker Ebrahim[a], Ali Gad[a], Sherif Kandil[a]

[a]*Department of Materials Science, Institute of Graduate Studies and Research, Alexandria University, 163 Horrya Avenue, El-Shatby, P.O. Box 832, Alexandria, Egypt, Tel. +201024604959; Fax: +2035603053; email: mohamedsaid@alexu.edu.eg (M. Said), Tel. +201021309751; Fax: +2034285792; email: shaker.ebrahim@alexu.edu.eg (S. Ebrahim), Tel. +201114454566; email: aligad2003@yahoo.com (A. Gad), Tel. +201003400746; email: s.kandil@usa.net (S. Kandil)*
[b]*Abu Qir Fertilizers and Chemical Industries Co., Postal Code: 21911, El-Tabyia, Rashid Road, Alexandria, Egypt*

Received 18 August 2016; Accepted 18 January 2017

ABSTRACT

Thin-film composite (TFC) membranes with polyamide (PA) as an active layer synthesized via interfacial polymerization (IP) are dominant in reverse osmosis (RO). This work reports the development of a TFC–PA–RO membrane that minimizes the energy consumption while maintaining superior membrane separation properties. The TFC–PA–RO membranes were prepared by IP of 2,6-diaminotoluene (DAT) and trimesoyl chloride (TMC) on polysulfone (PS) support. The conventional monomer, *m*-phenylenediamine, is replaced by a DAT monomer. These membranes were characterized by infrared spectroscopy, scanning electron microscope and contact angle measurements. It was found that the optimum preparation conditions for the TFC–PA–RO membranes included soaking DAT (1 wt%) for 2 min, TMC (0.15 wt%) for 0.5 min and curing at 75°C for 5 min. The TFC–PA–RO membrane prepared at these conditions exhibited a salt rejection of 99.54% and a permeate water flux of 11.4 L/m^2 h in 10 g/L NaCl feed solution at 18 bar. Also, the TFC–PA–RO membranes produced a salt rejection of 98.25% and a permeate water flux of 9.3 L/m^2 h at 35 bar in 35 g/L NaCl feed solution. This low operating pressure compared with the commercial membranes that operate at 55 bar for seawater desalination saves the energy consumed by the RO system to 1.29 kWh/m^3.

Keywords: Reverse osmosis; Polyamide; Thin-film composite; Membrane; Desalination

1. Introduction

Desalination using reverse osmosis (RO) technology has attracted immense interest as one of the solutions for producing reliable and sustainable water from seawater and brackish water [1]. The global expansion of seawater desalination and the associated excessive energy consumption have serious economic and environmental consequences. Therefore, the current RO development focused on reducing specific energy consumption (SEC), cost and addressing environmental concerns [2]. The minimum theoretical energy for seawater desalination with salt concentration of 35 g/L and 50% feedwater recovery is 1.06 kWh/m^3. The practical minimum energy consumption reported for an RO system is 1.58 kWh/m^3 for 50% water recovery of 35 g/L NaCl solution at 25°C, 100% NaCl rejection and 10.2 L/m^2 h flux, which indicates the need for further improvement [3].

Thin-film composite polyamide RO (TFC–PA–RO) membranes are currently the main class of RO membranes available in the market for water treatment and seawater desalination [4]. This is attributed to its high flux and high rejection that are provided by the thin aromatic polyamide (PA) separating layer [5]. Also, the chemistry and performance of the TFC layers can be independently optimized to maximize the membrane performance and stability [6].

* Corresponding author.

For most commercially available TFC–PA–RO membranes, the interfacial polymerization (IP) reaction takes place between *m*-phenylenediamine (MPD) and trimesoyl chloride (TMC) [7]. However, one of the major flaws in the current TFC–PA–RO membranes operation is the high energy consumption for pressurizing the seawater [8]. The applied pressure extends between 55 and 82 bar to provide sufficient driving force across the membrane for industrial production from seawater. The energy consumption of the primary feed pump for pressurizing the seawater accounts for a major portion of the total cost (80.6%) [9]. One of the most important attempts to improve the TFC–PA membranes performance and reduce SEC in RO processes is the development of new membranes based on novel monomers containing special functional groups [10,11].

In previous work, the TFC–PA–RO membranes prepared from the derivatives of MPD with electron donating group such as CH_3 and OCH_3 attached to the phenyl ring of MPD showed a better chlorine tolerance [12]. In this work, we prepared and characterized a TFC–PA–RO membrane with superior properties using 2,6-diaminotoluene (DAT) and TMC monomers. Important synthesis parameters, namely monomers concentration, reaction time and soaking time were considered influential factors that improve the flux. Moreover, the methyl group substituted on the aromatic diamine ring is considered as a bulky side group that inhibits the packing efficiency and produces a high free volume membrane with lower crystallinity. The high free volume in the membrane facilitates the permeation and consequently will lower the operating pressure and reduces the energy consumed by the primary feed pump [13]. The low energy consumption is reflected into lower operation and product costs. The water flux and salt rejection of the prepared RO membranes were assessed and carried out using a cross-flow cell.

2. Materials and methods

2.1. Materials

Polysulfone (PS; molecular weight 60,000, product of Acros Organics, USA) was used as a supporting material for the TFC–PA–RO membranes. *N*-Methylpyrrolidone (NMP; Fluka chemie, Switzerland) was used as a solvent. DAT (99%), MPD (99%) and TMC (98%) were supplied by Acros Company. *n*-Hexane (95%) was supplied by Tedia Company, USA. NaCl was supplied by MP Biomedical (France) to prepare the salt feed solution. The commercial RO membrane SW30-2540 was supplied by Dow Filmtec, USA.

2.2. Preparation of PS support membrane

PS pellets were dissolved in 72 mL of NMP with 18 wt%. This solution was mechanically stirred until the polymer was completely dissolved and then the solution was left to settle for 24 h to remove air bubbles. The solution was then casted on a clean glass plate using an autocasting machine (Zehntner 2300, Swiss) at constant spread speed of 10 mm/s and thickness of 250 μm. The cast membrane was immersed and coagulated in deionized water as the non-solvent at room temperature. The PS was gelled into a white microporous sheet and separated from the glass plate. The top surface of the PS (in contact with air) was used as a support surface for the TFC–PA–RO membrane deposition. The prepared PS membranes were then washed and moved to a new deionized water bath for at least 24 h until the solvent was removed.

2.3. Preparation of the TFC–PA–RO membrane

The PS support membranes were removed from deionized water and positioned onto a plastic plate. A rubber gasket and a plastic frame were placed on top of the support membrane. The plate membrane and gasket frame stack were held together by binder clips. The aqueous and organic solutions of the two monomers were prepared by dissolving DAT in deionized water and TMC in hexane, respectively. The aqueous solution was poured on the top surface of the PS support membrane to be soaked for 1, 2, 4 and 6 min. This residence time allowed DAT to penetrate into the pores of PS support membrane. Residual droplets of this aqueous solution were squeezed off using soft rubber roller to ensure that no visible aqueous droplets may form defects. Then, the TMC organic solution was poured on the PS support membrane for 0.25, 0.5, 1, 2 and 3 min, then the residual solution was drained and the stack was disassembled. The resulting membranes were cured at different curing temperatures and times. Finally, the prepared TFC–PA–RO membranes were immersed in deionized water until tested in cross-flow experiments.

2.4. Characterization techniques

2.4.1. Chemical structure: Fourier transform infrared spectroscopy

The chemical structure of PA membranes was characterized using Fourier transform infrared (FTIR; Perkin Elmer Spectrum BX-11 Infrared spectrometer FTIR LX 18-5255). The IR spectra were recorded in the range of wave number 4,000–400 cm^{-1} to determine the group frequencies and chemical structure of the prepared membranes.

2.4.2. Crystal structure: X-ray diffraction

X-ray diffraction (XRD) scans were carried out (using X-ray 7000 Shimadzu, Japan) at room temperature in the Bragg angle (2θ) in the range 10°–80° to determine the degree of crystallinity and interplanner distance of the prepared films. The X-ray source was a Cu target with settings of 30 kV and 30 mA, with scan speed 4°/min.

2.4.3. Morphology: scanning electron microscopy

Cross-sectional, surface and bottom images of the membranes were obtained using scanning electron microscopy (SEM-XL 30 JEOL). The morphological cross-section images of the PA membranes were snapped under liquid nitrogen to give a generally consistent and clean break. The membranes were sputter coated with thin film of gold. The membranes were mounted on a brass plate using double-sided adhesion tape in a lateral position. The thicknesses of the PA active layer were calculated from cross-section of SEM images using the Digimizer software.

2.4.4. Hydrophilicity: contact angle measurements

Surface hydrophilicity of the prepared membranes was evaluated from the average equilibrium sessile drop contact angles of deionized water on dried membrane surfaces. The contact angle of the TFC–PA–RO membranes surfaces was measured using Rame-Hart, Instrument Company, France. A drop of distilled water (2 μL) was placed on the RO membrane surface (3 cm × 2 cm) using a microsyringe (Hamilton Company, Reno, NV, USA). The liquid deposited on the solid surface, under gravity has a tendency to spread until the cohesion (internal forces) of the liquid, the gravity forces and the capillary (surface tension) forces are in balance, and an equilibrium state is reached. Once equilibrium is achieved (after 10–20 s) a contact angle between the solid surface and liquid can be measured. The contact angle was the average of five measurements at different positions on the surface within 10 s after the water drop was placed on the surface.

2.4.5. Membrane performance evaluation

The performance (salt rejection and water flux) was conducted for TFC–PA–RO membranes (area 42 cm^2) using cross-flow RO unit (CF042, Sterling, USA) with hydrolytic pump, pressure control valve and gauge through the rejection line, with variable frequency drive (SV015IG5A-4) and flow meter (F-550, USA). The tested membranes were cut with stainless steel cut die with dimension (8 × 11 cm) and were placed in stainless steel cell with the active layer facing the incoming feed with a feed flow rate of 1 L/min. Before the permeation tests, the membranes were kept at a constant operating pressure with deionized water for 1 h to obtain a steady flux and ensure a stable membrane. The water flux and salt rejection performance tests were conducted in NaCl of 10 and 35 g/L at feed pH of 7 ± 0.2 and temperature (25°C ± 1°C). The permeate flux was determined by measuring the volumetric permeate flow directly (L/m^2h). The determination of the total dissolved salt of permeate water was measured with a pH/conductivity meter (430 portable, Jenway, England). The salt rejection was calculated by applying the following equation [14]:

$$\text{Rejection}(\%) = 100 \times \frac{(C_f - C_p)}{C_f} \quad (1)$$

where C_f and C_p are the ionic conductivity of feed solution and permeate, respectively. The permeate water flux is defined as:

$$\text{Flux} = \frac{V}{A * t} \quad (2)$$

where V is the permeate volume (L), A is the membrane area (m^2) and t is the time (h).

3. Results and discussion

3.1. Mechanism of PA polymerization

In IP the two reacting monomers are dissolved in a pair of immiscible liquids. The aqueous phase contains DAT and acts as an acid acceptor extracting the hydrogen chloride by-product from the polymerization zone. The other organic phase consists of TMC that is dissolved in hexane. The IP reaction is initiated at the interface where the aqueous solution was impregnated in the PS support is brought into contact with the organic solution. An insoluble thin PA film is formed at the interface and grows in the organic side due to the negligible solubility of TMC in water and the good solubility of DAT in hexane. Hence, the IP reaction is mainly controlled by the diffusion of the DAT molecules to the reaction zone. Therefore, it is common to use a large excess of amine over acid chloride, which drives partitioning and diffusion of the amine into the organic phase [15]. The IP between DAT and TMC involves an incipient fast stage that forms a dense, highly cross-linked and ultrathin core of PA barrier layer followed by a slow growth stage that is DAT diffusion limited "self-limiting" [16]. The result of polymerization at this stage is the formation of a more loose second layer of PA which covers the core layer causing the ridge and valley morphology but having less effect on the membrane performance [17]. The use of trichloride increases the degree of cross-linking as initially the two monomers react to form linear chains as with the dichloride, while the third acyl chloride group can either undergo hydrolysis to form carboxylic acid or react with another diamine molecule to produce chain branching or cross-linking. The additional carboxyl group allows for a greater degree of cross-linking and when left unreacted it adds a mild anionic charge to the membrane at neutral pH [15]. The thickness and cross-link density of TFC membranes can be controlled by DAT diffusion and hydrolysis of TMC reactive sites. The IP reaction is terminated when the mass transfer resistance of the PA layer becomes great enough to prevent DAT transport into the organic phase [18]. The reaction scheme for the IP is shown in Fig. 1 where the PA contains a cross-linked portion (*Y*) and a more hydrophilic linear moiety (*X*) containing an unreacted acid chloride group that subsequently hydrolyzes to a carboxylic acid group.

3.2. The chemical structure of the PA layer

In order to identify the chemical structure of the active skin layer of the TFC–PA–RO membranes, FTIR spectra were recorded for TMC, DAT monomers and the PA layer as shown in Fig. 2. From the TMC spectrum, a peak at 1,755 cm^{-1} is characteristic of the C=O stretching vibration of the acid chloride moiety and a peak at 705 cm^{-1} is attributed to the C–Cl

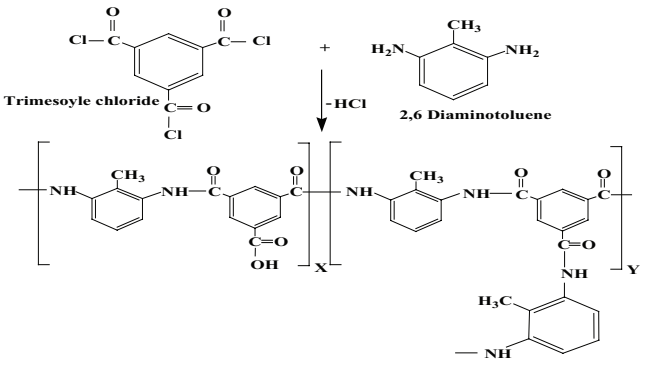

Fig. 1. A scheme for the proposed IP mechanism between DAT and TMC.

stretching vibrations [16–19]. The coupled doublet peak in the range of 3,410–3,334 cm^{-1} in the DAT spectrum is due to the N–H hydrogen bonded primary amine asymmetric and symmetrical stretching [20]. In the spectrum of PA, the broad peak at 3,477 cm^{-1} is attributed to the stretching vibration of the secondary amine groups (–NH) or hydroxyl groups (–OH) [21]. The C=O stretching vibration, amide I band, is shifted to lower frequency of absorption of 1,660 cm^{-1} due to additional conjugation in PA [21]. The conversion of a coupled doublet peak in the DAT spectrum to one broad peak, the shift of C=O in the TMC spectrum to lower frequency and the absence of C–Cl band in the PA spectrum, confirmed the formation of PA from the polymerization reaction of the DAT and TMC monomers. The appearance of amide II band of secondary amides at 1,570 cm^{-1} is attributed to the N–H bending of amide group (–CONH–) [20]. Secondary amide N–H wagging appears at 654 cm^{-1} [22]. The peak at 1,512 cm^{-1} is corresponding to the aromatic C=C bonds stretching vibration [22].

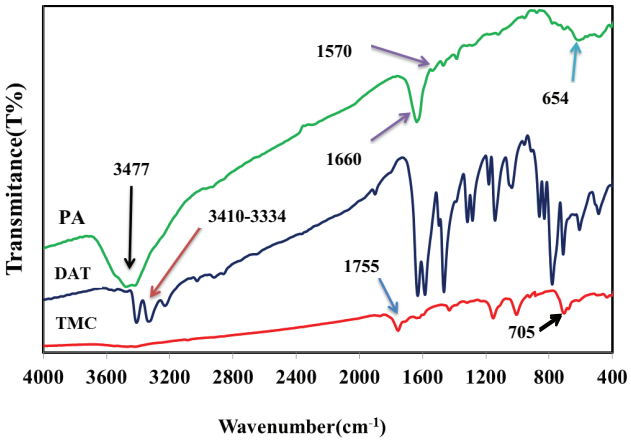

Fig. 2. FTIR spectra of TMC, DAT and PA.

3.3. PA structure studies using X-ray diffraction

XRD patterns of the TFC–PA–RO membranes prepared at 1 wt% of DAT or MPD for 2 min soaking time, 0.15 wt% of TMC for 0.5 min reaction time and at 75°C curing temperature for 5 min are shown in Fig. 3. The crystalline structures and interplanner distance of the PA-based DAT and MPD were characterized by XRD and compared. The two XRD diffraction patterns of the PA exhibited an amorphous broad peak around 2θ = 17.8°, which implies that the PA is amorphous in nature. There is no sharp peak which reveals a non-crystalline nature of PA. The XRD reflection peak of PA-based DAT was broader than based on MPD, suggesting the more amorphous nature. The *d*-spacing within the PA chains were calculated from XRD measurements as 5.128 and 5.087 Å for the PA-based DAT and MPD, respectively. The increase in free volume can be explained by the steric hindrance of the substituted methyl group, which results in an increase of the average chain distance and a decrease of the chain packing density [11–13].

3.4. Membrane morphology

SEM images were investigated to characterize the surface of the active skin layer, bottom and cross-section of the TFC–PA–RO membrane. Fig. 4 shows the SEM images for the TFC–PA–RO membranes prepared from 1 wt% of DAT for 2 min soaking time, 0.15 wt% TMC for 0.5 min reaction time and at 75°C curing temperature for 5 min. From the SEM surface photographs, Fig. 4(A), the PA skin layer appears dense rough and continuous with uniform ridge and valley morphology (the white part is the peak and the black part is the valley), which is characteristic of the PA membranes formed using an IP [23,24]. The thickness of the active PA skin layer was equal to about 0.466 μm and varied with different preparation condition. The bottom micrograph of the PS support layer has distinct porous structure with different pore diameter as shown in Fig. 4(B).

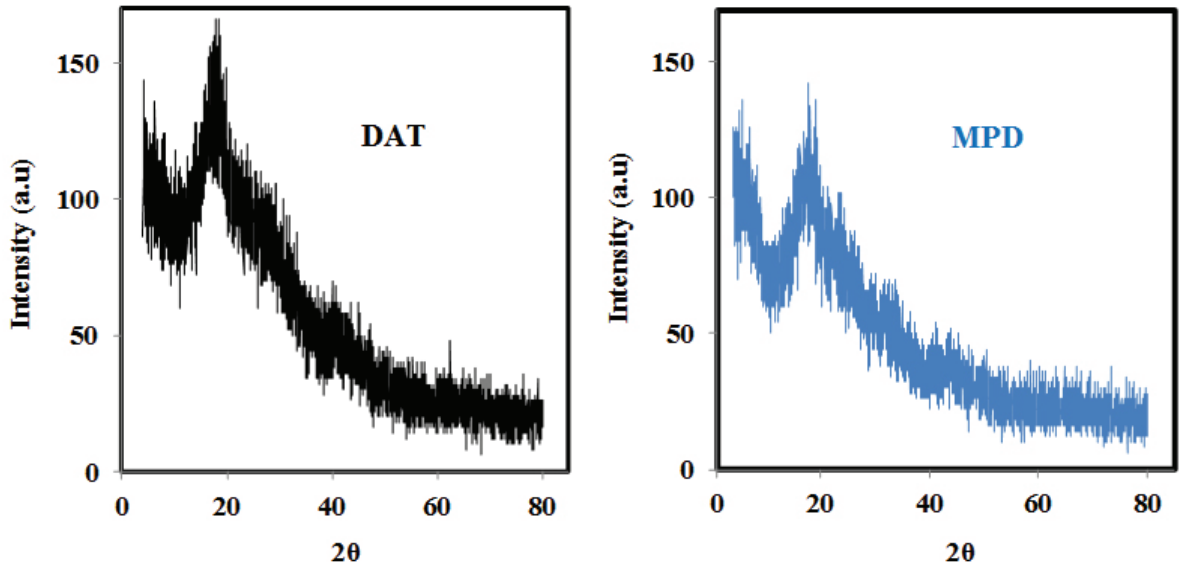

Fig. 3. XRD patterns of DAT- and MPD-based TFC–PA–RO membrane prepared at 1 wt% of DAT or MPD for 2 min soaking time, 0.15 wt% of TMC for 0.5 min reaction time and cured at 75°C for 5 min.

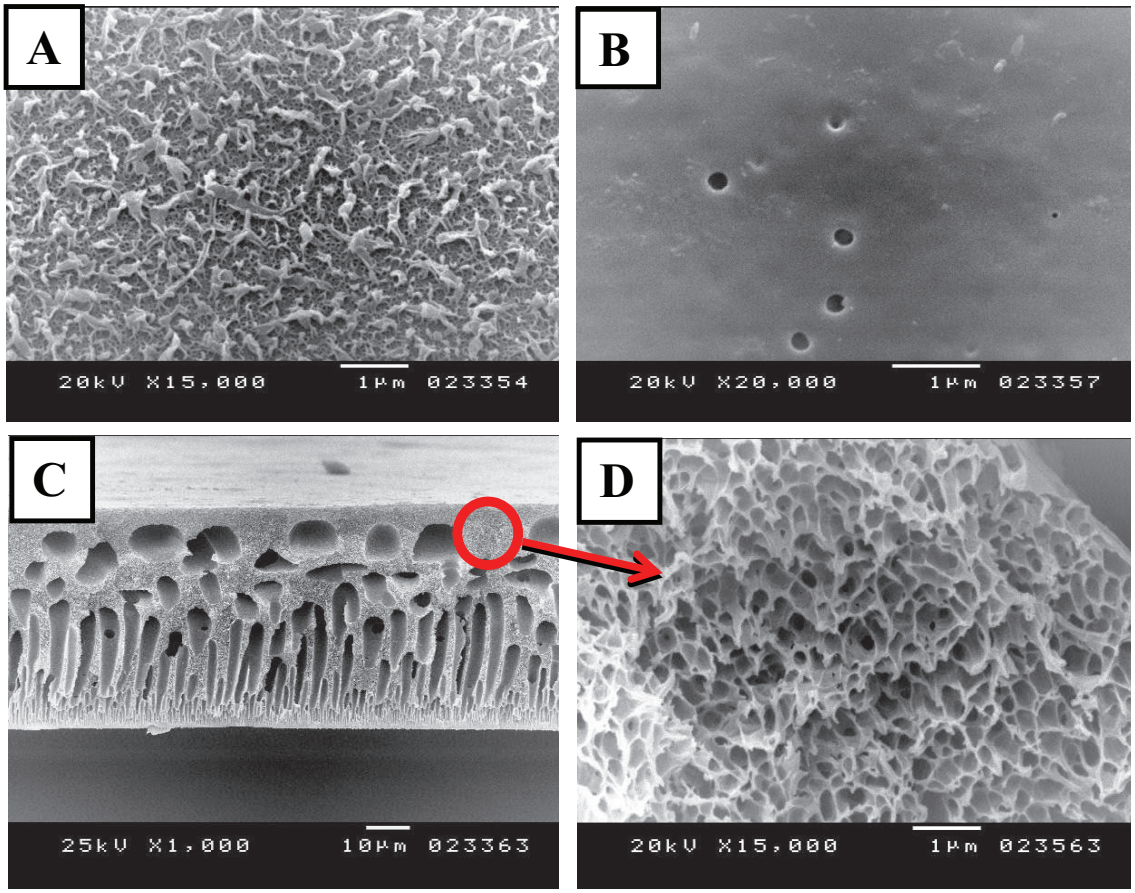

Fig. 4. SEM micrographs of: (A) surface, (B) bottom, (C) cross-section and (D) sponge-type structure of the TFC–PA–RO membrane prepared at 1 wt% of DAT for 2 min soaking time, 0.15 wt% of TMC for 0.25 min reaction time and at 75°C curing temperature for 5 min.

Fig. 4(C) shows the cross-section image of the TFC–PA–RO membrane with a dense skin layer at the surface and a porous structure underneath. At higher magnification the porous PS structure shows a sponge-type structure as shown in Fig. 4(D). The porous PS structure does not only have thin passage channels of increasing pore diameter from the top to the bottom side forming a finger-like morphology, but also have large pores penetrating the entire membrane cross-section. The channels structure decreases the resistance to mass transfer while the sponge-like morphology supports high pressure and favors the formation of an integral PA layer [24].

3.5. Hydrophilicity of PA–TFC–RO membranes

Hydrophilicity is an important property of RO membranes because the hydrophilic surface does not only increase the water permeate flux, but also reduces the membrane fouling. The lower the contact angle values indicate the higher hydrophilicity and a greater tendency for water to wet the material surface [25]. The hydrophilicity of the RO membrane is controlled by the electrostatic and/or hydrogen-bond interactions between the water molecules and surface functional groups. Because of the strong hydrogen-bond interactions between the adsorbed water molecules and the surface functional groups, the RO-membrane affinity to water molecules can be strengthened and the water droplet is prone to spread on the surface. The contact angle of the RO membrane is correspondingly decreased [26]. It was found that the contact angle of the PA membrane is smaller than the supporting PS film. This hydrophilicity is attributed to the presence of ionizable moieties of unreacted amines and carboxylic acids [27]. Fig. 5(A) shows the contact angle of TFC–PA–RO membranes prepared at different DAT concentrations for 2 min soaking time, 0.1 wt% of TMC for 1 min reaction time and at 75°C curing temperature for 5 min. It is noted that the contact angle has greatly increased at small concentration of DAT and steadily increases after 0.250 wt%. This may be attributed to the self-limiting of the interfacial reaction process. The contact angle increases from 34.69 to 55.45 with increasing of the DAT concentration from 0.065 to 2.5 wt%. With increasing of DAT concentration, the driving force for diffusion of DAT molecules is enhanced at the aqueous/organic interface producing PA film with high cross-linked units and lower contents of linear structure with pendant –COOH groups [27]. The effect of different soaking time on the contact angle is plotted in Fig. 5(B). The TFC–PA–RO membranes were prepared at a fixed DAT concentration of 1 wt%, 0.15 wt% of TMC for 0.5 min reaction time and at 75°C curing temperature for 5 min. Prolonging the soaking time from 1 to 6 min drives the contact angle to steadily increase from 37.5 to 60.8. This may be attributed to the fact

that extending the soaking time is similar to increasing of DAT concentration, which allows more DAT monomers to diffuse and penetrate through the PS porous structure. On the other hand, the effect of TMC concentrations on the contact angle contradicts with the DAT concentration as shown in Fig. 5(C). The TFC–PA–RO membranes were prepared at fixed DAT concentration of 1 wt% for 2 min soaking time, 1 min reaction time and at 75°C curing temperature for 5 min. Increasing the TMC concentrations from 0.04 to 0.22 wt%, resulted in a decline of the contact angle from 56.7 to 38.18. Excess of TMC concentrations provides large amounts of TMC molecules at the organic side of the interface where the PA thin film grows and results in more unreacted acid chloride groups and consequently higher contents of –COOH in the TFC membrane. The effect of the TMC reaction time on the membrane hydrophilicity is shown in Fig. 5(D). The TFC–PA–RO membranes were prepared at a fixed DAT concentration of 1 wt% for 2 min soaking time, 0.15 wt% of TMC at 75°C curing temperature for 5 min. The hydrophilicity of the TFC–PA–RO membranes was reduced with the increase of TMC reaction time. The short reaction time of 0.25 min produces membrane with lower contact angle of 33.3. The fast reaction rate results in membrane with lower degree of cross-linking and with more linear amide units with pendant acid groups. Extending the reaction time to 3 min causes extensive cross-linking and film growth with higher contact angle of 49.44. It can be seen that when the reaction time increases, the contact angle first sharply increased and then steadily increases. The small increase in the contact angle with increasing of the reaction time after 0.5 min implies that there is no sharp increase in the extent of cross-linking after such reaction time.

3.6. Membrane performance evaluation

The separation performance of the active PA layer depends not only on the overall film thickness, but also on the cross-link density of the internal structure. The cross-link density of the active PA layer is directly proportional to its crystallinity that is determined by the chain flexibility and the volume fraction of the polymer. The transport mechanism through a dense membrane is attributed to the molecular diffusion of permeates through the free volume fractions between the polymer chains [17]. The effect of the preparation parameters was studied to obtain an optimized set of conditions for the development of the PA–TFC membrane with the best RO performance.

3.6.1. Effect of DAT concentration

Fig. 6 depicts the effect of the operating pressure on the salt rejection and water flux of the TFC–PA–RO membranes prepared at different DAT concentrations in 10 g/L NaCl feed solution. The TFC–PA–RO membranes were prepared under different concentrations of DAT (0.0625, 0.125, 0.250, 0.5, 1, 2, 2.5 wt%) for 2 min soaking time, 0.1 wt% of TMC for 1 min reaction time and at 75°C curing temperature for 5 min. The experiment was conducted at 25°C and the pressure was varied from 16 bar to 26 bar to evaluate the TFC–PA–RO

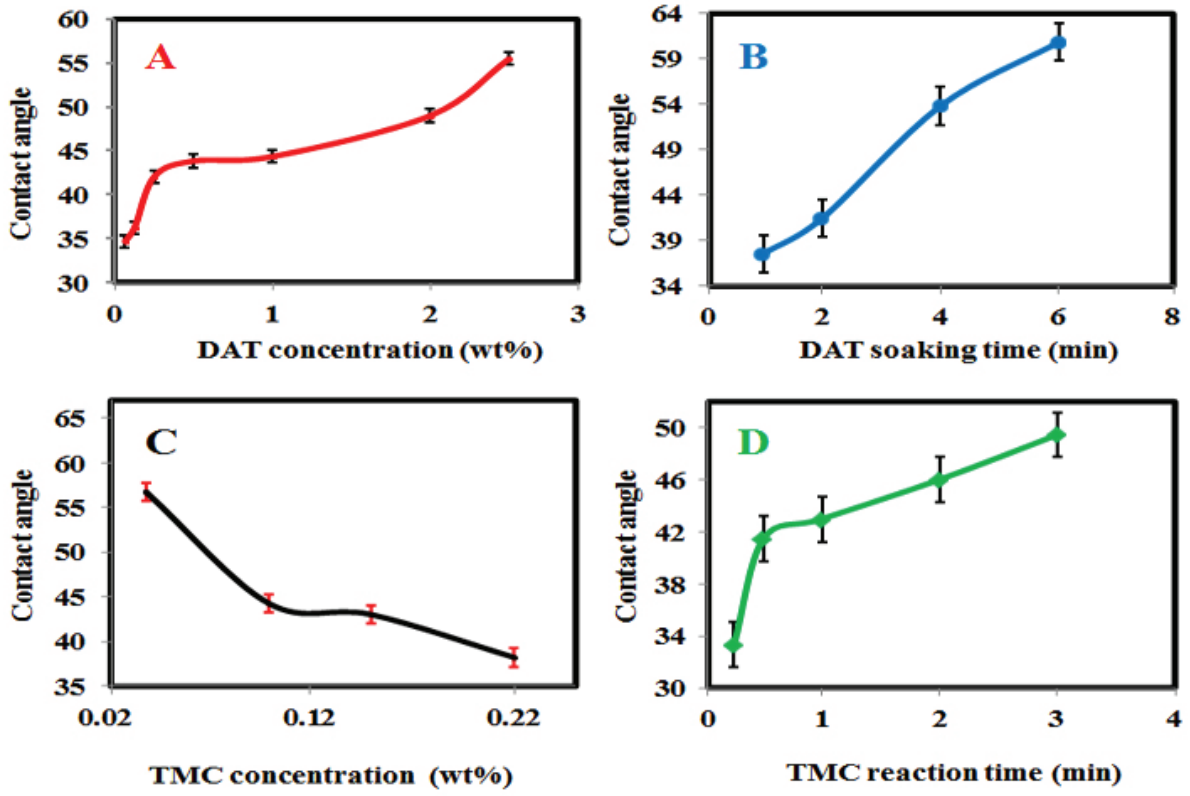

Fig. 5. Contact angles of TFC–PA–RO membranes prepared at different DAT concentrations (A), different DAT soaking times (B), different TMC concentrations (C) and different TMC reaction times (D).

membranes performance. It appeared from Fig. 6(A) that as the operating pressure increases from 16 bar to 26 bar, the salt rejection of the TFC membranes increases first until the pressure reaches 18 bar and then decreases at 20 bar. Compared with the MPD, the methyl side group in DAT monomer increases the fractional free volume in the PA active layer [11–13]. It has been reported that the mechanical strength of a membrane decreases with increasing the free volume [28,29]. The salt rejection is decreased again at pressure exceeding 20 bar due to the breakdown of the active layer structure which causing the membrane to permeate more water and salts. In addition, the decline of the salt rejection is may also be due to the increasing of the salt concentration difference on the two sides of the membrane [30]. The maximum operating pressure that ensures both mechanical and hydraulic stability is observed at 18 bar. The membrane prepared at 1 wt% of DAT exhibits the highest stability with increase of the operating pressure to 26 bar while the salt rejection decreases to 91% compared with other membranes. As might be anticipated from Fig. 6(B), a linear relationship exists between the flux and pressure over the measured range. The primary effect of increasing the operating pressure is to enhance the driving force which increases the water flux [31]. The water flux of the membrane prepared at 1 wt% DAT, increases from 6.2 to 13.5 L/m^2 h with increasing of the operating pressure from 16 to 26 bar. The low operating pressure of 18 bar is attributed to the increasing of interplanner distance within PA

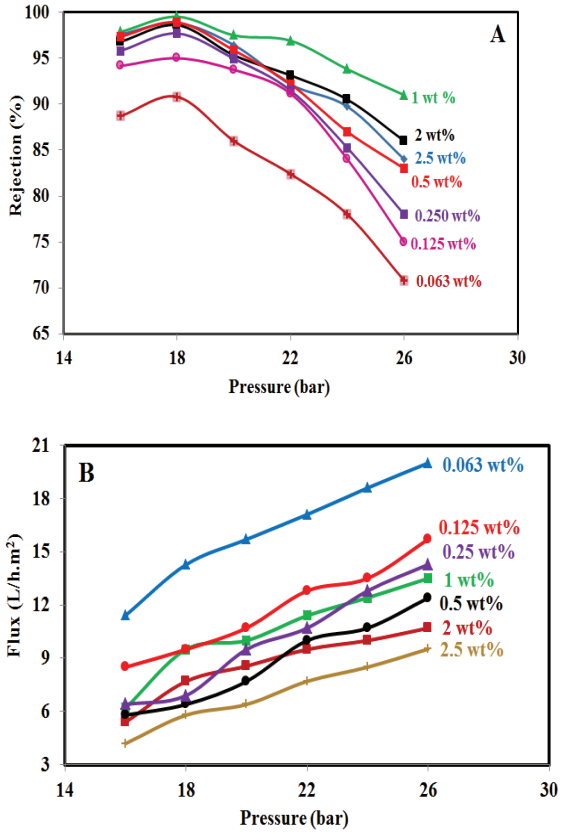

Fig. 6. Salt rejection (A) and water flux (B) of TFC–PA–RO membranes prepared at different DAT concentrations vs. operating pressure in 10 g/L NaCl feed solution.

chains caused by the bulky methyl group. Consequently, the energy consumed by the primary feed pump that accounts for the major portion of the energy consumption and the total desalination cost is reduced.

The salt rejection and water flux of the TFC–PA–RO membranes vs. the different DAT concentrations in 10 g/L NaCl feed solution at 18 bar are shown in Fig. 7. It is observed that the salt rejection improves by increasing the DAT concentration up to 1 wt% and further addition of DAT has a slight effect on the value of salt rejection. However, the permeate water flux is first sharply decreased with the increase of DAT concentration up to 0.5 wt% and then increases at 1 wt% and finally decreases steadily again at DAT concentrations higher than 1 wt%. The maximum salt rejection of 99.52% and water flux of 9.52 L/m^2 h were reached at 1 wt% of DAT optimum concentration. The separation performance of the active PA layer depends not only on the overall film thickness but also on the cross-link density of the internal structure [32]. At low concentration of DAT loose and less cross-linked PA layer is formed and permeates more water and salts [32]. However, higher DAT concentration the driving force for diffusion of DAT into the organic phase and leading to the formation of a dense and thick PA layer during the slow growth stage [33].

3.6.2. Effect of TMC concentration

The influence of the TMC concentrations on the TFC–PA–RO membrane salt rejection and permeate flux in 10 g/L NaCl feed solution at 18 bar is shown in Fig. 8. The TFC–PA–RO membranes were prepared at different TMC concentrations

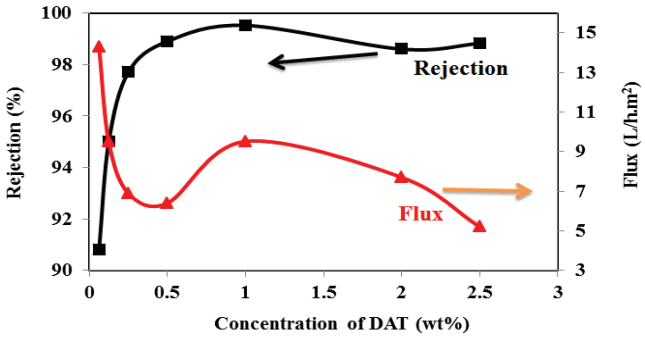

Fig. 7. Salt rejection and water flux of TFC–PA–RO membranes vs. DAT concentrations in 10 wt% NaCl feed solution at 18 bar.

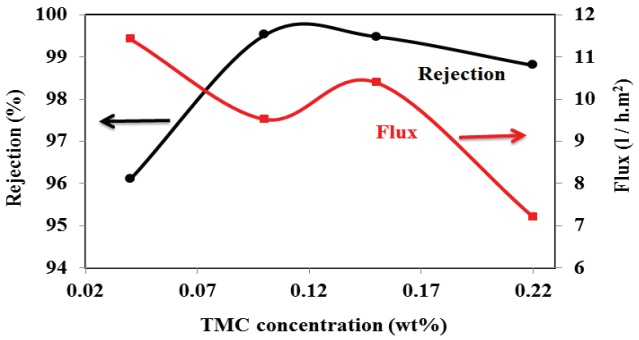

Fig. 8. Salt rejection and water flux of TFC–PA–RO membranes vs. TMC concentrations in 10 wt% NaCl feed solution at 18 bar.

(0.04, 0.1, 0.15, 0.22 wt%) for 1 min reaction time, 1 wt% of DAT for 2 min soaking time and at 75°C curing temperature for 5 min. The salt rejection rises from 96.1% to 99.48% with increasing the TMC concentration from 0.04 to 0.15 wt% and then the salt rejection slightly changed above this concentration. However, the water flux decreased from 11.4 to 7.2 L/m² h with increasing the TMC concentration from 0.04 to 0.22 wt%, respectively. The TFC membrane prepared at 0.15 wt% of TMC exhibits the highest salt rejection of 99.48% and water flux of 10.39 L/m² h suggests the formation of thin, more hydrophilic and defect free PA layer. At low TMC concentration, the degree of polymerization is expected to be lower because of the insufficient concentration of TMC at the interfacial reaction zone. Consequently, the formed PA skin layer was less cross-linked, thin and loose and it poorly rejects NaCl while permeates more water. The formation of hydrophilic, thick, dense and compact top PA layer, at higher TMC concentrations, reduces the water flux and slightly changes the salt rejection [31].

3.6.3. Effect of TMC reaction time

Fig. 9 displays the effect of TMC reaction time on the TFC–PA–RO performance in 10 wt% NaCl feed solution at 18 bar. The PA–RO–TFC membranes were prepared at fixed DAT concentration of 1 wt% for 2 min soaking time, 0.15 wt% of TMC at 75°C curing temperature for 5 min. The polymerization reaction is very fast. At short reaction time (0.25 min), the membrane has salt rejection of 95.8% and water flux of 11.8 L/m² h. The PA chains have not enough time to get properly organized in short reaction times resulting in a less cross-linked and opened PA layer, which could explain the high permeate flux and low salt rejection [32]. Increasing of the TMC reaction time to 0.5 min, the water flux is slightly decreased to 11.4 L/m² h while the salt rejection is increased to 99.54%. However, rising of this time to 3 min, the salt rejection is slightly changed whereas water flux is dramatically declined to 5.7 L/m² h. This may be attributed to the increasing of PA layer thickness with extending the reaction time. After a certain period of reaction, the water flux and salt rejection will almost stay constant because both of the thickness and compactness of the selective skin layer are almost fixed [31]. The optimum TMC reaction time is chosen to be 0.5 min.

3.6.4. Effect of DAT soaking time

Fig. 10 indicates the effect of DAT soaking time on the salt rejection and water flux of TFC–PA–RO membranes in 10 wt% NaCl feed solution at 18 bar. The TFC–PA–RO membranes were prepared at fixed DAT concentration of 1 wt%, 0.15 wt% of TMC for 0.5 min reaction time and cured at 75°C for 5 min. It is found that the salt rejection increases with increasing of the DAT soaking time from 1 to 2 min and further longer soaking times have a slight effect on the salt rejection. On the other hand, the increasing of DAT soaking time reduces the water flux from 12.5 L/m² h at 1 min to 7.14 L/m² h at 6 min. The longer soaking time enhances the amount of DAT that diffused and penetrated the PS support layer pores forming thick and cross-linked PA film. The membrane prepared at 2 min DAT soaking time exhibits the maximum salt rejection of 99.54% and water flux of 11.42 L/m² h.

3.7. Comparison of the membranes performance and their energy consumption

The preparation conditions were systematically studied and optimized to give the highest membranes performance. The optimum conditions were 1 wt% of DAT for 2 min soaking time, 0.15 wt% of TMC for 0.5 min reaction time and curing at 75°C for 5 min. The performance of the DAT and MPD-based TFC–PA–RO membranes are compared in 35 g/L NaCl feed solution (seawater) as shown in Fig. 11. The MPD-based TFC–PA–RO membrane was prepared at 1 wt% of MPD for 2 min soaking time, 0.15 wt% of TMC for 0.5 min reaction time and curing at 75°C for 5 min. The performance of the two membranes shows the same trend. The maximum salt rejection of 98.25% and water flux of 9.3 L/m² h are observed at 35 bar for DAT-based membrane. On the other hand, the MPD-based membrane shows a maximum salt rejection of 97.24% and water flux of 15.7 L/m2 h at 55 bar. In previous experiment, the optimum conditions for preparation of MPD-based TFC–PA–RO membrane were soaking at 2 wt% of MPD for 2 min, 0.1 wt% of TMC for 1 min reaction time and curing at 70°C for 5 min. The membrane prepared at this condition has a maximum salt rejection of 96% and water flux of 5 L/m² h at 55 bar.

The performance of both DAT-based TFC–PA–RO membrane and the commercial TFC–PA–RO membrane (SW30-2540) is compared in 10 g/L NaCl feed solution as shown in Fig. 12. It is noted that the DAT-based membrane has higher salt rejection but lower water flux than the commercial membrane. However, the TFC–PA–RO membrane based on DAT shows a maximum salt rejection and water flux at 18 bar while the commercial membrane operates at 50 bar.

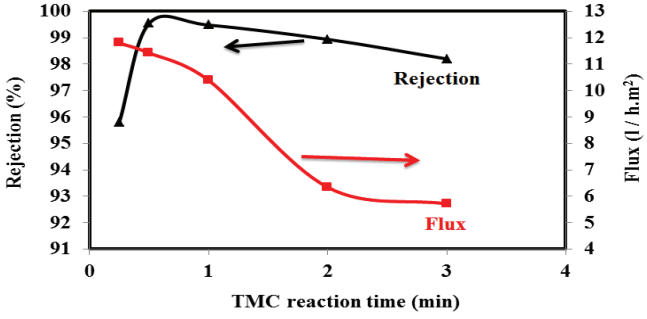

Fig. 9. Salt rejection and water flux of TFC–PA–RO membranes vs. TMC reaction times in 10 wt% NaCl feed solution at 18 bar.

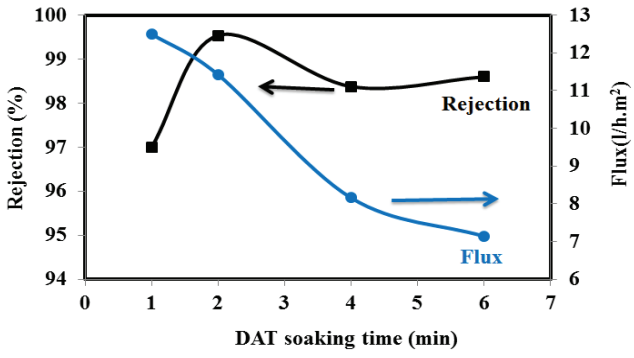

Fig. 10. Salt rejection and water flux of TFC–PA–RO membranes vs. DAT soaking times in 10 wt% NaCl feed solution at 18 bar.

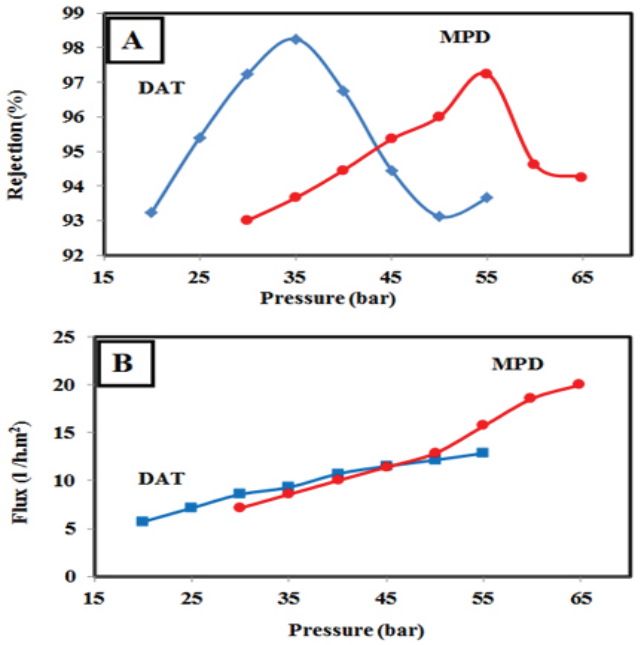

Fig. 11. Salt rejection (A) and water flux (B) of TFC–PA–RO membranes based on DAT and MPD vs. operating pressure in 35 g/L NaCl feed solution.

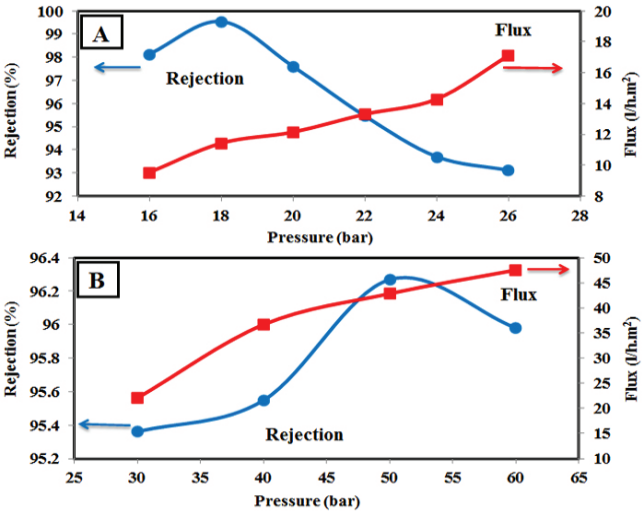

Fig. 12. Salt rejection and water flux of TFC–PA–RO membrane based on DAT (A) and the commercial TFC–PA–RO membrane (SW30-2540) (B) vs. operating pressure in 10 g/L NaCl feed solution.

The commercial membrane shows a salt rejection of 97% and water flux of 20 L/m² h in 35 g/L NaCl feed solution at 55 bar. The DAT-based membrane has higher salt rejection (98.25%) with lower water flux (9.3 L/m² h) but operates at lower pressure (35 bar) than the commercial membrane.

The SEC of the pump is calculated from the following equation [7]:

$$\mathrm{SEC}_{\mathrm{pump}} = \frac{W_{\mathrm{pump}}}{Q_p} = \frac{Q_f \Delta P}{Q_p} \quad (3)$$

where W_{pump} is the pump work (w), Q_f is the feed flow rate (L/min), Q_p is the permeate flow rate (L/min) and ΔP is the transmembrane pressure difference (bar).

The total energy consumption for an RO system using TFC–PA–RO membrane based on DAT is 1.29 kWh/m³ for 35 g/L NaCl solution at 25°C, 98.25% NaCl rejection and 9.3 L/m² h permeate flux. On the other hand, the MPD-based TFC–PA–RO membrane prepared at the same condition consumes 1.74 kWh/m³ for 35 g/L NaCl solution at 25°C, 97.24% NaCl rejection and 15.7 L/m² h permeate flux. However, the TFC–PA–RO membrane prepared at optimum MPD condition consumes 3.57 kWh/m³ for 35 g/L NaCl solution at 25°C, 96% NaCl rejection and 5 L/m² h permeate flux. It can be concluded that the TFC–PA–RO membrane based on DAT monomer not only rejects more salts but also consumes lower energy than the MPD-based and commercial membrane for brackish water and seawater desalination. Also, this membrane has lower energy consumption by 21% compared with the practical minimum energy consumption reported for RO system [4].

4. Conclusions

A TFC–PA–RO membrane was prepared through the IP of DAT onto porous PS support membrane. The optimal polymerization conditions for the TFC–PA–RO membrane were as follows: DAT = 1.0 wt%; soaking time = 2 min; TMC = 0.15 wt%; reaction time = 0.5 min; curing temperature = 75°C; curing time = 5 min. The desired TFC–PA–RO membrane fabricated under the optimized preparation conditions has a typical salt rejection of 98.25% and a water flux of 9.3 L/m² h for a feed solution of 35 g/L NaCl at 35 bar. The systematic performance studies showed that the TFC membrane prepared in this work operates at a low pressure of 35 bar compared with 55–82 bar for most of commercially TFC–PA–RO membranes while maintaining almost the same quality. The lower operating pressure can account for reduction of the energy consumption, costs and environmental consequences in water industry. The DAT-based membrane has lower energy consumption than the MPD-based membrane and the practical minimum energy consumption reported for the RO system. The water flux obtained in this work is relatively low and needs to be further improved for commercial application. Further studies will be made in the future to improve the water flux while maintaining or even increasing the salt rejection.

Acknowledgment

The authors acknowledge the Science and Technology Development Fund in Egypt for supporting this project (project ID 3988).

References

[1] D. Xevgenos, K. Moustakas, D. Malamis, M. Loizidou, An overview on desalination & sustainability: renewable energy-driven desalination and brine management, Desal. Wat. Treat., 57 (2014) 2304–2314.
[2] A. Yechiel, Y. Sheva, Optimization of energy costs for SWRO desalination plants, Desal. Wat. Treat., 46 (2012) 304–311.
[3] A. Subramani, J.G. Jacangelo, Emerging desalination technologies for water treatment: a critical review, Water Res., 75 (2015) 164–187.

[4] M. Ding, A. Ghoufi, A. Szymczyk, Molecular simulations of polyamide reverse osmosis membranes, Desalination, 343 (2014) 48–53.
[5] W. Gao, F. She, J. Zhang, L.F. Dumée, L. He, P.D. Hodgson, L. Kong, Understanding water and ion transport behavior and permeability through poly(amide) thin film composite membrane, J. Membr. Sci., 487 (2015) 32–39.
[6] M. Liu, Z. Chen, S. Yu, D. Wu, C. Gao, Thin-film composite polyamide reverse osmosis membranes with improved acid stability and chlorine resistance by coating N-isopropylacrylamide-co-acrylamide copolymers, Desalination, 270 (2011) 248–257.
[7] M. Ding, A. Szymczyk, F. Goujon, A. Soldera, A. Ghoufi, Structure and dynamics of water confined in a polyamide reverse-osmosis membrane: a molecular-simulation study, J. Membr. Sci., 458 (2014) 236–244.
[8] D. Kim, G.L. Amy, T. Karanfil, Disinfection by-product formation during seawater desalination: a review, Water Res., 81 (2015) 343–355.
[9] Y. Ghalavand, M.S. Hatamipour, A. Rahimi, A review on energy consumption of desalination processes, Desal. Wat. Treat., 54 (2015) 1526–1541.
[10] J. Espeso, A.E. Lozano, J.G. de la Campa, J. de Abajo, Effect of substituents on the permeation properties of polyamide membranes, J. Membr. Sci., 280 (2006) 659–665.
[11] D. Mohan, L. Kullova, A study on the relationship between preparation condition and properties/performance of polyamide TFC membrane by IR, DSC, TGA, and SEM techniques, Desal. Wat. Treat., 51 (2013) 586–596.
[12] S. Son, J. Jegal, Preparation and characterization of polyamide reverse-osmosis membranes with good chlorine tolerance, J. Appl. Polym. Sci., 120 (2011) 1245–1252.
[13] K. Chang, Y. Huang, K. Lee, K. Tung, Free volume and polymeric structure analyses of aromatic polyamide membranes: a molecular simulation and experimental study, J. Membr. Sci., 354 (2010) 93–100.
[14] S.H. Kim, S.Y. Kwak, T. Suzuki, Positron annihilation spectroscopic evidence to demonstrate the flux enhancement mechanism in morphology controlled thin film composite (TFC) membrane, Environ. Sci. Technol., 39 (2005) 1764–1771.
[15] M. Liu, D. Wu, S. Yu, C. Gao, Influence of the polyacyl chloride structure on the reverse osmosis performance, surface properties and chlorine stability of the thin-film composite polyamide membranes, J. Membr. Sci., 326 (2009) 205–214.
[16] A.M.A. El-Aassar, Polyamide thin film composite membranes using interfacial polymerization: synthesis, characterization and reverse osmosis performance for water desalination, Aust. J. Basic Appl. Sci., 6 (2012) 382–391.
[17] B. Khorshidi, T. Thundat, B.A. Fleck, M. Sadrzadeh, Thin film composite polyamide membranes: parametric study on the influence of synthesis conditions, RSC Adv., 5 (2015) 54985–54997.
[18] J. Lee, A. Hill, S. Kentish, Formation of a thick aromatic polyamide membrane by interfacial polymerisation, Sep. Purif. Technol., 104 (2013) 276–283.
[19] J. Coates, Interpretation of Infrared Spectra, A Practical Approach, R.A. Meyers, Ed., Encyclopedia of Analytical Chemistry: Applications, Theory and Instrumentation, 1st ed., Vol. 2, John Wiley & Sons Ltd, Chichester, 2000, pp. 10815–10837.
[20] B.H. Stuart, Infrared Spectroscopy: Fundamentals and Applications, John Wiley & Sons, Ltd, University of Technology, Sydney, Australia, 2004.
[21] Z. Zhang, S. Wang, H. Chen, Q. Liu, J. Wang, T. Wang, Preparation of polyamide membranes with improved chlorine resistance by bis-2,6-N,N-(2-hydroxyethyl) diaminotoluene and trimesoyl chloride, Desalination, 331 (2013) 16–25.
[22] A. Soroush, J. Barzin, M. Barikani, M. Fathizadeh, Interfacially polymerized polyamide thin film composite membranes: preparation, characterization and performance evaluation, Desalination, 287 (2012) 310–316.
[23] E.M. Vrijenhoek, S. Hong, M. Elimelech, Influence of membrane surface properties on initial rate of colloidal fouling of reverse osmosis and nanofiltration membranes, J. Membr. Sci., 188 (2001) 115–128.
[24] N.Y. Yip, A. Tiraferri, W.A. Phillip, J.D. Schiffman, M. Elimelech, High performance thin film composite forward osmosis membrane, Environ. Sci. Technol., 44 (2010) 3812–3818.
[25] Y. Jin, Z. Sua, Effects of polymerization conditions on hydrophilic groups in aromatic polyamide thin films, J. Membr. Sci., 330 (2009) 175–179.
[26] Q. Li, X. Pan, Z. Qu, X. Zhao, Y. Jin, H. Dai, B. Yang, X. Wang, Understanding the dependence of contact angles of commercially RO membranes on external conditions and surface features, Desalination, 309 (2013) 38–45.
[27] O. Coronell, B. Marinas, X. Zhang, D.G. Cahill, Quantification of functional groups and modeling of their ionization behavior in the active layer of FT30 reverse osmosis membrane, Environ. Sci. Technol., 42 (2008) 5260–5266.
[28] L. Brinkert, N. Abidine, P. Aptel, On the relation between compaction and mechanical properties for ultrafiltration hollow fibers, J. Membr. Sci., 77 (1993) 123–131.
[29] Y.A. Hussain, M.H. Al-Saleh, S.S. Ar-Ratrout, The effect of active layer non-uniformity on the flux and compaction of TFC membranes, Desalination, 328 (2013) 17–23.
[30] M. Liu, S. Yu, Q. Ming, Q. Pan, C. Gao, Impact of manufacture technique on seawater desalination performance of thin-film composite polyamide-urethane reverse osmosis membranes and their spiral wound elements, J. Membr. Sci., 348 (2010) 268–276.
[31] M. Liu, S. Yu, J. Tao, C. Gao, Preparation, structure characteristics and separation properties of thin-film composite polyamide-urethane seawater reverse osmosis membrane, J. Membr. Sci., 325 (2008) 947–956.
[32] S. Hermans, H. Mariën, E. Dom, R. Bernstein, I.F.J. Vankelecom, Simplified synthesis route for interfacially polymerized polyamide membranes, J. Membr. Sci., 451 (2014) 148–156.
[33] H. Zhu, A. Szymczyk, B. Balannec, On the salt rejection properties of nanofiltration polyamide membranes formed by interfacial polymerization, J. Membr. Sci., 379 (2011) 215–223.